



# Evaluation of Perkin Elmer Amorphous Silicon Electronic Portal Imaging Device for Small Photon Field Dosimetry

Mohammad Haghparast (PhD)<sup>1,2</sup>, Wrya Parwaie (PhD)<sup>3</sup>,  
Mohsen Bakhshandeh (PhD)<sup>4</sup>, Nina Tuncel (PhD)<sup>5</sup>, Seied Rabi  
Mahdavi (PhD)<sup>1\*</sup>

## ABSTRACT

**Background:** Electronic portal imaging devices (EPIDs) are applied to measure the dose and verify patients' position.

**Objective:** The present study aims to evaluate the performance of EPID for measuring dosimetric parameters in small photon fields.

**Material and Methods:** In this experimental study, the output factors and beam profiles were obtained using the amorphous silicon (a-Si) EPID for square field sizes ranging from  $1 \times 1$  to  $10 \times 10$  cm<sup>2</sup> at energies 6 and 18 mega-voltage (MV). For comparison, the dosimetric parameters were measured with the pinpoint, diode, and Semiflex dosimeters. Additionally, the Monaco treatment planning system was selected to calculate the output factors and beam profiles.

**Results:** There was a significant difference between the output factors measured using the EPID and that measured with the other dosimeters for field sizes lower than  $8 \times 8$  cm<sup>2</sup>. In the energy of 6 MV, the gamma passing rates (3%/3 mm) between EPID and diode profile were 98%, 98%, 95%, 94%, 93%, and 94% for  $1 \times 1$ ,  $2 \times 2$ ,  $3 \times 3$ ,  $4 \times 4$ ,  $5 \times 5$ , and  $10 \times 10$  cm<sup>2</sup>, respectively. The measured penumbra width with EPID was higher compared to that measured by the diode dosimeter for both energies.

**Conclusion:** The EPID can measure the dosimetric parameters in small photon fields, especially for beam profiles and penumbra measurements.

## Keywords

Computer-Assisted; Electronic Portal Imaging Device; Photons; Radiation Dosimetry; Radiotherapy Planning; Small Field

## Introduction

Radiation therapy is increasingly used for the treatment of cancer patients [1]. The goal of radiation therapy is to kill malignant cells while preserving normal cells [2], i.e. the prescribed dose for tumors is restricted by the tolerance of the organs to save the critical organs. In some conditions, the prescribed dose to tumor volumes is restricted by the radiation tolerance of the critical organs [3]. New techniques, such as stereotactic radiosurgery (SRS), intensity-modulated radiotherapy (IMRT), and volumetric modulated arc therapy (VMAT) result in decreasing doses in organs at risk [4]. In these modern techniques, small fields are used for highly conformed dose distributions [5].

<sup>1</sup>Department of Medical Physics, School of Medicine, Iran University of Medical Sciences, Tehran, Iran

<sup>2</sup>Department of Radiology, Faculty of Para-Medicine, Hormozgan University of Medical Sciences, Bandare-Abbas, Iran

<sup>3</sup>Department of Medical Physics, Faculty of Paramedical Sciences, Ilam University of Medical Sciences, Ilam, Iran

<sup>4</sup>Department of Radiology Technology, School of Allied Medical Sciences, Shahid Beheshti University of Medical Science, Tehran, Iran

<sup>5</sup>Radiation Oncology Department, School of Medicine, Akdeniz University, Antalya, Turkey

\*Corresponding author:  
Seied Rabi Mahdavi  
Department of Medical Physics, School of Medicine, Iran University of Medical Sciences, Tehran, Iran  
E-mail: srmahdavi@hotmail.com

Received: 26 December 2021  
Accepted: 29 January 2022

At least one of the three conditions: 1) the lack of lateral charged particle equilibrium, 2) partial occlusion of the radiation source, and 3) larger or equal to the size of the detector with the beam dimensions, is essential for small fields [6]. Small radiation fields are defined at a dimension smaller than  $4 \times 4 \text{ cm}^2$  [7]. The small field dosimetry is associated with some complicated issues, as follows: 1) lateral electronic disequilibrium (LED), 2) volume averaging effect, partial occlusion of the radiation source, and 3) the steep gradient of the radiation field and the lack of a reference dosimeter to measure the relative dosimetric parameters such as percentage depth dose (PDD) and beam profiles [8]. These challenges can lead to the transfer of inaccurate data to treatment planning systems during commissioning since the known dosimeters have at least one disadvantage. The volume averaging effect is important for ion chambers [9]; diodes are energy-dependent [10], and metal oxide–silicon semiconductor field-effect transistor (MOS-FET) is angular dependent [11]. Therefore, a dosimeter with good performance is desired in small photon fields [8].

Electronic portal imaging devices (EPIDs) were originally introduced as a tool for verifying patients' positions [12]. Current amorphous-silicon EPIDs possess special features leading to their utilization for alternative purposes, such as patient-specific quality assurance and dose measurements [13]. In addition, EPIDs are an invaluable asset in treatment procedures due to their performance as an in-vivo dosimeter [14]. However, some studies have examined the performance of EPID in the dosimetry of conventional fields [15, 16], and little effort has been made to evaluate the performance of this tool in small field dosimetry.

The present study aimed to evaluate the performance of EPID in measuring dosimetric parameters in small photon fields. Since no ideal dosimeter is defined for measurement of dose in the small fields, the measured data us-

ing EPID were compared with data measured by pinpoint, diode, and semi-flex dosimeters. The dosimetric parameters were computed with the treatment planning system (TPS) to compare measured data.

## Material and Methods

In this experimental study, a linear accelerator (Elekta synergy platform linac system) with photon beam energies of 6 and 18 MV was used, equipped with amorphous silicon (a-Si) EPID and a multileaf collimator system, with 40 leaf pairs. The flat-panel of EPID was a Perkin-Elmer XRD 1640 detector with specifications, as follows: 1) active imaging area of  $41 \times 41 \text{ cm}^2$ , 2) matrix size of  $1024 \times 1024$  pixels, and 3) pixel size of 0.4 mm; the X-ray imaging software (XIS, US, version 3.2) was used to acquire the imaging data. Other detectors used, are pinpoint (model 31016, volume of  $0.016 \text{ cm}^3$ , PTW company, Germany), Semiflex (model 31010, volume of  $0.125 \text{ cm}^3$ , PTW company, Germany), and diode (Type E, model 60017, volume of  $0.03 \text{ mm}^3$ , PTW, Germany). Commissioned Monaco treatment planning system was used for calculated data.

### EPID calibration

EPID was calibrated based on Elekta protocol before imaging to eliminate background noise and achieve a spatially uniform response. First, a dark field is acquired by averaging frames without any radiation to obtain the background pixel value. These measured pixel values were assumed as an offset and subtracted from all image frame acquisition. In the next step, the difference between the pixel sensitivities was determined via the flood field acquired by the uniform irradiation of the field over the entire active area. Finally, the EPID dosimetry system was calibrated using delivering a known dose to the EPID and a relationship between the pixel value and the dose.

### Dose linearity measurement

The dose linearity of Linac was confirmed

via a PTW MP3 water phantom, and a Farmer ion chamber and imaging were performed in an open field of  $10 \times 10 \text{ cm}^2$  with different monitor units (MU) from 20 to 200 MU in 20 MU steps. For each image, a region-of-interest (ROI) in the dimension of  $10 \times 10 \text{ mm}^2$  was selected at the center of the image. For a certain field, the pixel values were measured in mentioned ROI for all frames and averaged. In the next step, the sum of the average values was considered as the pixel value of that field; finally, the pixel value versus MU was drawn.

### Output factor measurement

The collimator scatter factors were measured behind the build-up region at depths of 2.08 cm and 3.26 cm for 6 and 18 MV, respectively. A slab with a water-equivalent thickness of 1.18 cm and an intrinsic buildup of EPID (9 mm) were placed on EPID for 6 MV. Two slabs were placed on the EPID surface to measure the collimator scatter factors at a depth of 3.26 cm and an energy of 18 MV. In addition, the slab layers (water-equivalent thickness of 10 cm) were placed upon EPID to measure total output factors; irradiation and imaging were conducted with 100 MU for square field sizes ranging from  $1 \times 1$  to  $10 \times 10 \text{ cm}^2$  ( $1 \times 1$ ,  $2 \times 2$ ,  $3 \times 3$ ,  $4 \times 4$ ,  $5 \times 5$ ,  $8 \times 8$ , and  $10 \times 10 \text{ cm}^2$ ). For each field size, the pixel values were determined by a certain ROI. Both collimator scatters and total output factors were calculated by normalizing the measured pixel value from each field size to that measured from the reference field size ( $10 \times 10 \text{ cm}^2$ ). The output factors were obtained for two energies 6 and 18 MV, separately.

The output factors were measured using pinpoint, Semiflex, and diode detectors for similar conditions (field sizes, depth, energies, and source-detector distances (SDD)) with EPID. The collimator scatter factors and total output factor were obtained in the air and water phantom (dimension:  $30 \times 30 \times 30 \text{ cm}^3$ ), respectively. Appropriate brass build-up caps were used for each above-mentioned dosimeter to determine

collimator scatter factors. In addition, a virtual water phantom was defined in Monaco software (version 5.11) to measure the total output factor with TPS. In the next step, a point dose was measured and the dose was calculated for each above-mentioned field size at the depth of 10 cm three times to minimize measurement errors. Other conditions (energies and SSD) were selected similar to what was reported above.

### Beam profile measurement

The detective layer of EPID was set to 160 cm from the source for beam profile measurements. The water equivalent slabs with appropriate thickness were placed on EPID so that the active layer was placed at a depth of 10 cm; images were obtained with 100 MU irradiation for square field sizes ranging from  $1 \times 1$  to  $10 \times 10 \text{ cm}^2$  ( $1 \times 1$ ,  $2 \times 2$ ,  $3 \times 3$ ,  $4 \times 4$ ,  $5 \times 5$ , and  $10 \times 10 \text{ cm}^2$ ). The beam profiles are obtained in the central frame at an SDD of 160 cm. For each field size, the pixel values were calculated in the cross-plane (right-left). The in-plane profiles were not reported in the present work due to good agreement with the cross-plane profiles. All pixel values were normalized to the central axis pixel value (by multiplying by 100) to calculate the beam profiles, measured for two energies 6 and 18 MV, separately.

The beam profile curves were constructed using three detectors (pinpoint, Semiflex, and diode) for similar conditions (field sizes, depth, energies, direction, and SSD) with EPID. All beam profiles were performed with PTW MP3 water phantom and MEPHYSTO software. A virtual water phantom was defined and doses were measured at the cross-plane direction to measure the beam profiles using TPS; these data were read in VeriSoft software, version 7.1 (PTW, Freiburg, Germany). All conditions were selected similar to what was reported above. The beam profiles were compared using the gamma index method with criteria of 3% for dose difference and 3 mm for distance to an agreement; further, each measurement

was performed three times to achieve high precision.

### Results

In Figure 1, the EPID response versus the different monitor units (MU) was shown for two energies 6 and 18 MV. The slope and linear correlation coefficient of the linearity curve were 30066 and 0.9999, for energies 6 MV and 31438 and 0.9998, for energies 6 MV, respectively.

The measured total output factor ( $S_{c,p}$ ) using EPID, Semiflex, pinpoint, diode, and TPS at two energies of 6 and 18 MV are shown in Figures 2a and b, respectively. For 6 MV, The differences between EPID and diode were 11.9, 10.7, 8.9, 10.4, 9.6, and 3.9% in the 1×1, 2×2, 3×3, 4×4, 5×5, and 8×8 cm<sup>2</sup> field sizes, respectively. For the 18 MV photon beam, these differences were obtained 13.2, 12.2, 8.6, 6.2, 4.1, and 1.3% for the 1×1, 2×2, 3×3, 4×4, 5×5, and 8×8 cm<sup>2</sup> field sizes, respective-

ly. The maximum difference between all measurements was 34.6% between the diode and pinpoint in 1×1 cm<sup>2</sup> field size at energy 6 MV.

The measured collimator scatter factor using EPID for 6 and 18 MV photon beams were compared with corresponding output factors of Semiflex, pinpoint, and diode as seen in Figures 3a and b, respectively. The result shows that the difference between EPID and diode were 12.9, 10.6, 10.2, 7.8, 6.1, and 0.1% in the 1×1, 2×2, 3×3, 4×4, 5×5, and 8×8 cm<sup>2</sup> field sizes, respectively, in 6 MV energy. Furthermore, for energy 18 MV, the above-mentioned differences were obtained 15.6, 13.7, 9.4, 6.3, 5.2, and 1.6% for the 1×1, 2×2, 3×3, 4×4, 5×5, and 8×8 cm<sup>2</sup> field sizes, respectively.

Figures 4 and 5 demonstrate the beam profiles measured with EPID, pinpoint, diode, and Semiflex and calculated with TPS at a depth of 10 cm for 6 MV and 18 MV. In the energy 6 MV, the gamma passing rates (3%/3mm) between EPID and diode profiles were 98, 98,

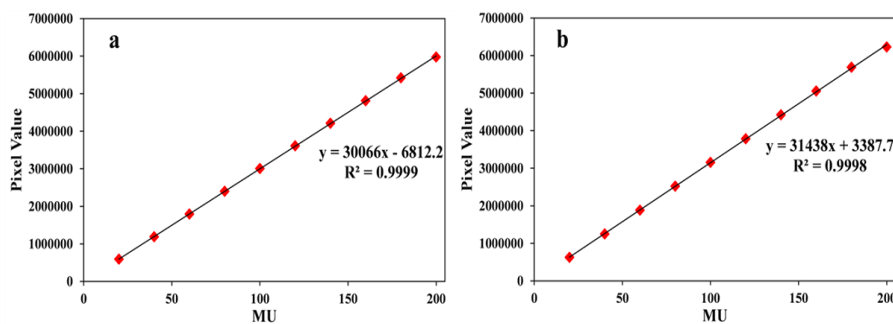


**Figure 1:** Electronic portal imaging devices (EPID) response to different monitor unit (MU) for two energies. a)6 MV and b)18 MV

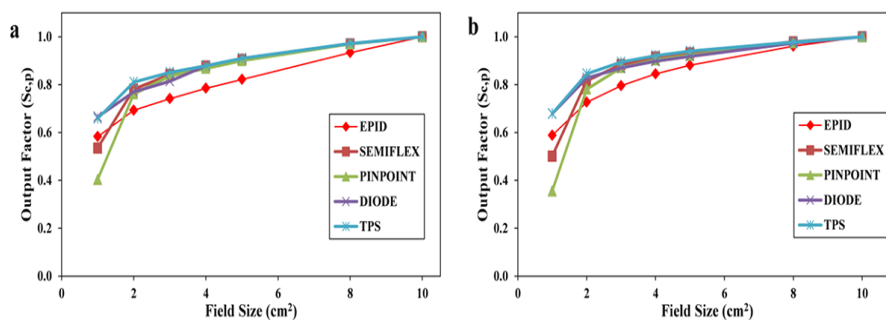


**Figure 2:** Measured total output factor ( $S_{c,p}$ ) for two energies. a)6 MV and b)18 MV.

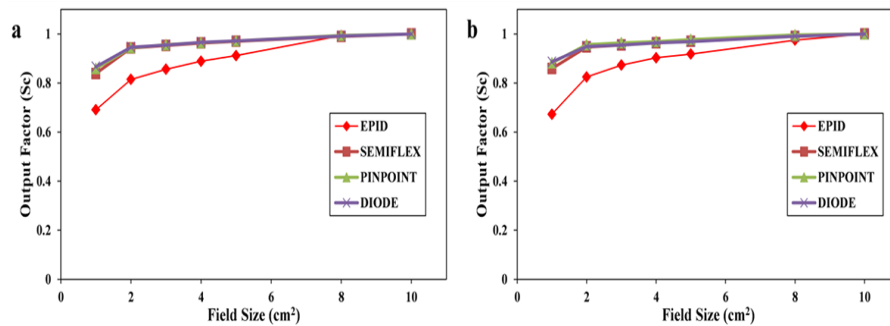


**Figure 3:** Measured collimator scatter factor ( $S_c$ ) for two energies. a) 6 MV and b) 18 MV.

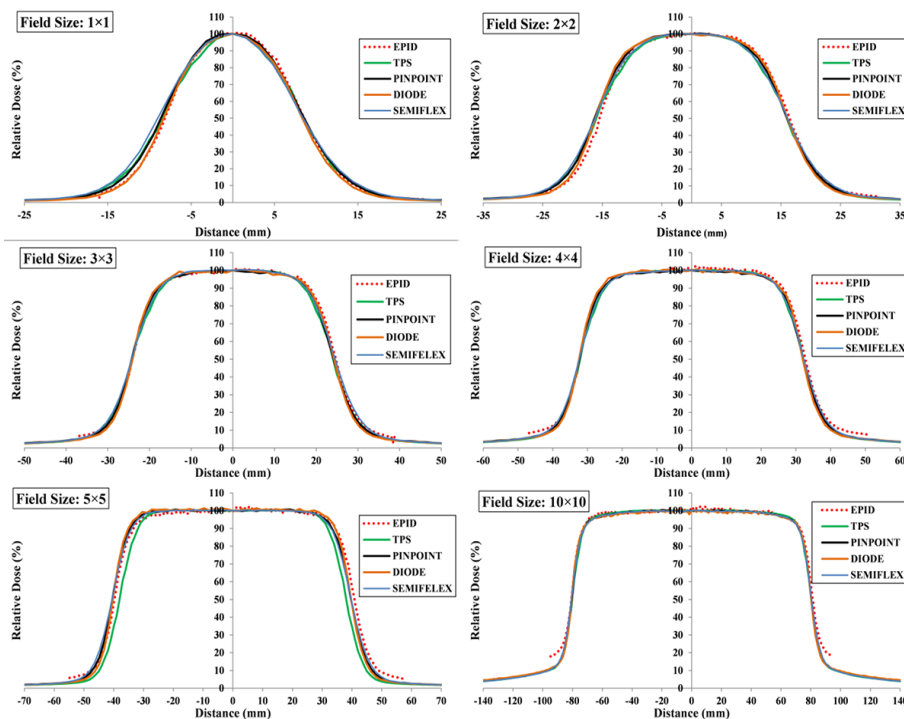


**Figure 4:** Measured beam profiles at depth=10 cm and beam energy=6 MV for field sizes 1×1, 2×2, 3×3, 4×4, 5×5 and, 10×10 cm<sup>2</sup>.

95, 94, 93, and 94% for 1×1, 2×2, 3×3, 4×4, 5×5, and 10×10 cm<sup>2</sup>, respectively. Furthermore, for 18 MV, these passing rate indexes were calculated at 98, 97, 96, 97, 94, and 93% for 1×1, 2×2, 3×3, 4×4, 5×5, and 10×10 cm<sup>2</sup>, respectively.

The penumbra widths (80%-20%) and field sizes at SDD of 160 cm were measured with EPID, pinpoint, diode, and Semiflex at 10 cm depth and energy of 6 MV for actual field sizes

of 1×1, 2×2, 3×3, 4×4, 5×5, and 10×10 cm<sup>2</sup>. Accordingly, these data were compared with calculated penumbra obtained from TPS as seen in Table 1. It is evident that the ratio of penumbra to field size decreased as field size increased. Table 2 highlights the measured and calculated penumbra widths (80%-20%) for 1×1, 2×2, 3×3, 4×4, 5×5, and 10×10 cm<sup>2</sup> field sizes at the depth of 10 cm and energy of 18 MV.

## Discussion

Advanced radiotherapy techniques, such as SRS, Stereotactic body radiation therapy (SBRT), IMRT, and VMAT are widely used due to better therapeutic ratios and need verification dosimetrically before applying even during treatment. The advanced techniques are based on small fields; however, dosimetry of small fields is associated with some

challenges, such as charged particle disequilibrium, volume averaging effect, and partial occlusion of the radiation source. Different radiotherapy centers use different devices; EPID can be a tool for pre-treatment verification and in-vivo dosimetry, in addition to its main role as a patient position verification tool. In the present study, the performance of EPID was evaluated to measure the dosimetric parameters, such as

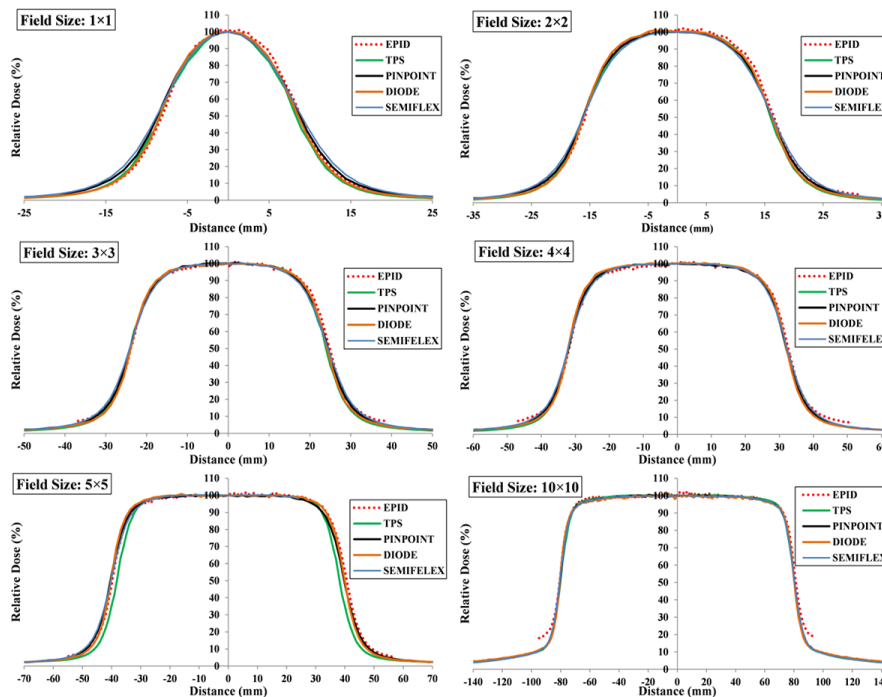


**Figure 5:** Measured beam profiles at depth=10 cm and beam energy=18 MV for field sizes 1×1, 2×2, 3×3, 4×4, 5×5 and, 10×10 cm<sup>2</sup>.

**Table 1:** Measured penumbra widths (80%-20%) for six field sizes 1×1, 2×2, 3×3, 4×4, 5×5, and 10×10 cm<sup>2</sup> at the beam energy 6 MV and depth of 10 cm.

Actual Field Size (cm <sup>2</sup> )	Measured field size (cm)					Penumbra widths (80%-20%) (cm)				
	EPID	Semiflex	Pinpont 3D	Diode	TPS	EPID	Semiflex	PinPoint 3D	Diode	TPS
1×1	1.64	1.74	1.72	1.66	1.60	0.60	0.70	0.65	0.60	0.70
2×2	3.20	3.24	3.23	3.23	3.20	0.72	0.85	0.77	0.67	0.80
3×3	4.88	4.88	4.84	4.83	4.80	0.76	0.89	0.79	0.74	0.90
4×4	6.48	6.46	6.44	6.44	6.40	0.84	0.93	0.83	0.75	1.00
5×5	8.08	8.07	8.05	8.05	8.00	0.90	0.96	0.87	0.78	1.00
10×10	16.20	16.13	16.08	16.10	16.00	1.07	1.00	1.00	0.94	1.05

EPID: Electronic Portal Imaging Devices, TPS: Treatment Planning System

**Table 2:** Measured penumbra widths (80%-20%) for six field sizes 1×1, 2×2, 3×3, 4×4, 5×5, and 10×10 cm<sup>2</sup> at the beam energy 18 MV and depth of 10 cm.

Actual Field Size (cm <sup>2</sup> )	Measured field size (cm)					Penumbra widths (80%-20%) (cm)				
	EPID	Semiflex	Pinpoint 3D	Diode	TPS	EPID	Semiflex	PinPoint 3D	Diode	TPS
1×1	1.68	1.77	1.74	1.70	1.60	0.60	0.74	0.67	0.61	0.70
2×2	3.24	3.25	3.24	3.23	3.30	0.76	0.90	0.80	0.72	0.80
3×3	4.88	4.86	4.85	4.81	4.80	0.84	0.95	0.85	0.78	0.80
4×4	6.44	6.45	6.41	6.43	6.40	0.90	1.00	0.90	0.80	0.88
5×5	8.04	8.05	8.02	8.02	8.00	1.00	1.00	0.93	0.85	0.90
10×10	16.10	16.10	16.08	16.08	16.00	1.12	1.10	1.00	0.92	0.96

EPID: Electronic Portal Imaging Devices, TPS: Treatment Planning System

output factor and beam profiles at field sizes ranging from 1×1 to 10×10 cm<sup>2</sup>.

As shown in Figure 1, the EPID exhibits a linear response in the range of 20 to 200 MU. In the current study, the high correlation coefficient squared ( $r^2$ ) shows the presented portal imaging system with a good linearity response, which is one of the essential properties of a dosimetry system. The presented results demonstrate similar behavior for two energies of 6 and 18 MV. The obtained results are consistent with those of Grządziel et al. that evaluated the performance of EPID as a pre-treatment verification tool in IMRT [17].

As seen in Figures 2 and 3, the total output factors and collimator scatter factors were measured using EPID, pinpoint, diode, and Semiflex for some field sizes at two energies and compared with TPS data. In the field sizes equal to and lower than 4×4 cm<sup>2</sup>, a significant difference was considered between the obtained output factors using EPID and 3 other dosimeters. The main reason could be the selected ROI size. The number of pixels adjacent to the central axis pixel affecting the output factor measurement increased as the size of ROI increased. Consequently, the uncertainty in the measurement of output factors increased, especially for small fields. Another reason for the difference between output factors measured using EPID and 3 other do-

simeters is the detector positioning errors, playing the main role in measuring the output factors at small photon fields with a bell-shaped profile [18].

Figures 2 and 3 revealed that the output factor measured with diode is higher than that measured using EPID, pinpoint, and Semiflex, due to the inherent overresponse of the diode dosimeter. As field size increases, the inherent over response of the diode also increased because of the containing high-density materials [18], leading to the output factor measured using the diode associated with uncertainty. Therefore, a diode is not a suitable tool for output factor measurement in small fields with sizes lower than 2×2 cm<sup>2</sup> [18].

For field sizes lower than 4×4 cm<sup>2</sup>, the beam profiles obtained with EPID were in better agreement with the diode and pinpoint measurements than those measured by the Semiflex and calculated using TPS due to the close size of pixels at EPID (0.4 mm) to the active volume of the diode and pinpoint detector with 0.03 mm<sup>3</sup> 0.016 cm<sup>3</sup>, respectively. The pixel size of EPID is significantly lower than the active volumes of Semiflex with 0.125 cm<sup>3</sup>. One of the main challenges in small field dosimetry is the steep gradient of the radiation field. In this situation, an ideal dosimeter should have a good spatial resolution. Therefore, EPID and diodes have better perfor-

mance in measuring the beam profiles due to lower pixel size. Increasing field size results in decreasing the difference between the measured profiles. Accordingly, in field sizes equal to and larger than  $4 \times 4 \text{ cm}^2$ , no noticeable difference was between the obtained beam profiles using EPID and 3 other dosimeters. The reason for this behavior is the reduction of dose gradient and decreasing of lateral electron disequilibrium with increasing field size.

In Tables 1 and 2, the penumbra widths (80%-20%) were measured using EPID, pinpoint, diode, and Semiflex for several field sizes at two energies and compared with TPS calculated penumbra. According to obtained results, the diode detector showed the lowest penumbra due to its small pixel size. The penumbra width measured using EPID is in better agreement with the diode and pinpoint measurements than those measured with Semiflex because of pixels of almost the same size. The Semiflex demonstrated the highest penumbra width compared to the others in the current study, due to the volume averaging effect in small field dosimetry using detectors with large sensitive volumes. Some studies reported that the volume averaging effect causes the penumbra broadening [19, 20]. In addition, the results showed that the ratio of penumbra width to field size decreases with increasing field size since partial occlusion of radiation source reduced with increasing the field size [21,22].

The flatness and symmetry parameters were extracted from the beam profiles at a depth of 10 cm for both energies. Analysis of the data revealed no significant difference between the measured and calculated flatness and symmetry. Finally, our finding is consistent with that of Ding *et al.* who evaluated the flatness and symmetry parameters using EPID and various detectors [23].

## Conclusion

In the present study, the performance of EPID was evaluated for measuring output fac-

tors and profiles of small fields for two-photon energies of 6 and 18 MV. The EPID showed a linear response in the range of 20 to 200 MU for both energies of 6 and 18 MV. A notable difference was seen between the obtained output factors using EPID and other dosimeters for field sizes equal to and lower than  $4 \times 4 \text{ cm}^2$ . In addition, the beam profiles obtained with EPID were in better agreement with the diode measurements than those measured by the pinpoint and Semiflex, due to the close size of pixels at EPID to the active volume of the diode. Overall, EPID is a valuable tool to measure the dosimetric parameters in small photon fields, especially for beam profiles and penumbra measurements.

## Authors' Contribution

SR. Mahdavi conceived the idea. The paper was written by M. Haghparast and W. Parwaie. M. Bakhshandeh and N. Tuncel gather data and the related literature and also help with writing the related works. The method implementation was conducted by M. Haghparast. Analysis was conducted by W. Parwaie. The research work was proofread and supervised by SR. Mahdavi. All the authors read, modified, and approved the final version of the manuscript.

## Ethical Approval

The Ethics Committee of Akdeniz University approved the protocol of the study (Ethic cod: KAEK-659).

## Funding

This study was supported as a research project under grant number 16843 by the Iran University of Medical Sciences, Tehran, Iran.

## Conflict of Interest

None

## References

1. Wang K, Tepper JE. Radiation therapy-associated toxicity: Etiology, management, and prevention. *CA Cancer J Clin.* 2021;**71**(5):437-54. doi: 10.3322/caac.21689. PubMed PMID: 34255347.
2. Castelli J, Simon A, Acosta O, Haigrón P,



- Nassef M, Henry O, et al. The role of imaging in adaptive radiotherapy for head and neck cancer. *IRBM*. 2014;**35**(1):33-40. doi: 10.1016/j.irbm.2013.12.003.
3. Taylor A, Powell ME. Intensity-modulated radiotherapy--what is it? *Cancer Imaging*. 2004;**4**(2):68-73. doi: 10.1102/1470-7330.2004.0003. PubMed PMID: 18250011. PubMed PMCID: PMC1434586.
  4. Eekers DBP, Roelofs E, Cubillos-Mesías M, Niël C, Smeenk RJ, Hoeben A, et al. Intensity-modulated proton therapy decreases dose to organs at risk in low-grade glioma patients: results of a multicentric in silico ROCOCO trial. *Acta Oncol*. 2019;**58**(1):57-65. doi: 10.1080/0284186X.2018.1529424. PubMed PMID: 30474448.
  5. Parwaie W, Geraily G, Shirazi A, Yarahmadi M, Shakeri A, Ardekani MA. Evaluation of lung heterogeneity effects on dosimetric parameters in small photon fields using MAGIC polymer gel, Gafchromic film, and Monte Carlo simulation. *Appl Radiat Isot*. 2020;**166**:109233. doi: 10.1016/j.apradiiso.2020.109233. PubMed PMID: 32836165.
  6. Palmans H, Andreo P, Huq MS, Seuntjens J, Christaki KE, Meghzifene A. Dosimetry of small static fields used in external photon beam radiotherapy: Summary of TRS-483, the IAEA-AAPM international Code of Practice for reference and relative dose determination. *Med Phys*. 2018;**45**(11):e1123-e45. doi: 10.1002/mp.13208. PubMed PMID: 30247757.
  7. Aspradakis MM, Byrne JP, Palmans H, Duane S, Conway J, Warrington AP, Rosser K. IPEM Report 103: Small field MV photon dosimetry. Report Number, IAEA-CN--182; International Atomic Energy Agency (IAEA); 2010.
  8. Parwaie W, Refahi S, Ardekani MA, Farhood B. Different Dosimeters/Detectors Used in Small-Field Dosimetry: Pros and Cons. *J Med Signals Sens*. 2018;**8**(3):195-203. doi: 10.4103/jmss.JMSS\_3\_18. PubMed PMID: 30181968. PubMed PMCID: PMC6116321.
  9. Würfel JU. Dose measurements in small fields. *Med Phys*. 2013;**1**(1):81-90.
  10. Eklund K, Ahnesjö A. Modeling silicon diode dose response factors for small photon fields. *Phys Med Biol*. 2010;**55**(24):7411-23. doi: 10.1088/0031-9155/55/24/002. PubMed PMID: 21098913.
  11. Kumar AS, Sharma SD, Ravindran BP. Characteristics of mobile MOSFET dosimetry system for megavoltage photon beams. *J Med Phys*. 2014;**39**(3):142-9. doi: 10.4103/0971-6203.139002. PubMed PMID: 25190992. PubMed PMCID: PMC4154181.
  12. Ford EC, Chang J, Mueller K, Sidhu K, Todor D, Mageras G, Yorke E, Ling CC, Amols H. Cone-beam CT with megavoltage beams and an amorphous silicon electronic portal imaging device: Potential for verification of radiotherapy of lung cancer. *Medical Physics*. 2002;**29**(12):2913-24. doi: 10.1118/1.1517614.
  13. Van Elmpt W, McDermott L, Nijsten S, Wendling M, Lambin P, Mijnheer B. A literature review of electronic portal imaging for radiotherapy dosimetry. *Radiother Oncol*. 2008;**88**(3):289-309. doi: 10.1016/j.radonc.2008.07.008. PubMed PMID: 18706727.
  14. Celi S, Costa E, Wessels C, Mazal A, Fourquet A, Francois P. EPID based in vivo dosimetry system: clinical experience and results. *J Appl Clin Med Phys*. 2016;**17**(3):262-76. doi: 10.1120/jacmp.v17i3.6070. PubMed PMID: 27167283. PubMed PMCID: PMC5690938.
  15. Vial P, Greer PB, Hunt P, Oliver L, Baldock C. The impact of MLC transmitted radiation on EPID dosimetry for dynamic MLC beams. *Med Phys*. 2008;**35**(4):1267-77. doi: 10.1118/1.2885368. PubMed PMID: 18491519.
  16. Olaciregui-Ruiz I, Vivas-Maiques B, Kaas J, Perik T, Wittkamper F, Mijnheer B, Mans A. Transit and non-transit 3D EPID dosimetry versus detector arrays for patient specific QA. *J Appl Clin Med Phys*. 2019;**20**(6):79-90. doi: 10.1002/acm2.12610. PubMed PMID: 31083776. PubMed PMCID: PMC6560233.
  17. Grządziel A, Smolińska B, Rutkowski R, Ślosarek K. EPID dosimetry—configuration and pre-treatment IMRT verification. *Reports of Practical Oncology & Radiotherapy*. 2007;**12**(6):307-12. doi:10.1016/S1507-1367(10)60069-7.
  18. Charles PH, Cranmer-Sargison G, Thwaites DI, Crowe SB, Kairn T, Knight RT, Kenny J, Langton CM, Trapp JV. A practical and theoretical definition of very small field size for radiotherapy output factor measurements. *Med Phys*. 2014;**41**(4):041707. doi: 10.1118/1.4868461. PubMed PMID: 24694127.
  19. Godson HF, Ravikumar M, Sathiyam S, Ganesh KM, Ponmalar YR, Varatharaj C. Analysis of small field percent depth dose and profiles: Comparison of measurements with various detectors and effects of detector orientation with different jaw settings. *J Med Phys*. 2016;**41**(1):12-20. doi: 10.4103/0971-6203.177284. PubMed PMID: 27051165. PubMed PMCID: PMC4795411.
  20. Pappas E, Maris TG, Zacharopoulou F, Papadakis A, Manolopoulos S, Green S, Wojnecki C. Small

- SRS photon field profile dosimetry performed using a PinPoint air ion chamber, a diamond detector, a novel silicon-diode array (DOSI), and polymer gel dosimetry. Analysis and intercomparison. *Med Phys.* 2008;**35**(10):4640-8. doi: 10.1118/1.2977829. PubMed PMID: 18975710.
21. Chand B, Kumar M, Kumar M. Comprehensive Review Of Small Field Dosimetry. *European Journal of Molecular & Clinical Medicine.* 2020;**7**(7):3595-607.
22. Agarwal A, Rastogi N, Maria Das KJ, Yoganathan SA, Udayakumar D, Kumar S. Investigating the Electronic Portal Imaging Device for Small Radiation Field Measurements. *J Med Phys.* 2017;**42**(2):59-64. doi: 10.4103/jmp.JMP\_131\_16. PubMed PMID: 28706350. PubMed PMCID: PMC5496271.
23. Ding A, Xing L, Han B. Development of an accurate EPID-based output measurement and dosimetric verification tool for electron beam therapy. *Med Phys.* 2015;**42**(7):4190-8. doi: 10.1118/1.4922400. PubMed PMID: 26133618. PubMed PMCID: PMC4474956.